Letter

Topological transport of vorticity on curved magnetic membranes

Chau Dao,[1] Ji Zou,[2] Eric Kleinherbers,[1] and Yaroslav Tserkovnyak[1]
[1]*Department of Physics and Astronomy and Bhaumik Institute for Theoretical Physics, University of California, Los Angeles, California 90095, USA*
[2]*Department of Physics, University of Basel, Klingelbergstrasse 82, CH-4056 Basel, Switzerland*

(Received 2 November 2023; revised 21 October 2024; accepted 27 January 2025; published 3 March 2025)

In this work, we study the transport of vorticity on curved dynamical two-dimensional magnetic membranes. We find that topological transport can be controlled by geometrically reducing symmetries, enabling processes absent from flat magnetic systems. To this end, the vorticity 3-current is constructed, which obeys a continuity equation immune to local disturbances of the magnetic texture and spatiotemporal fluctuations of the membrane. We show how electric current can manipulate vortex transport in geometrically nontrivial magnetic systems. As an illustrative example, we propose a minimal setup that realizes an experimentally feasible energy storage device and discuss its thermodynamic efficiency in terms of a *vortexoelectric* counterpart of the thermoelectric figure of merit ZT.

DOI: 10.1103/PhysRevB.111.L100401

Introduction. Much progress has been made both theoretically and experimentally in understanding, engineering, and driving topological magnetic textures [1–12]. This has resulted in numerous proposals that exploit spin texture topology for technological applications, such as domain wall and skyrmion racetracks [13–17], energy storage [18–20], long-range signal transport [21–29], and quantum information processing [30–32]. The utility of these spin structures is rooted in the metastability of topological excitations and the variety of ways to manipulate them [4,11,33–35]. To foster the development of these technologies, it is crucial to innovate avenues to drive topological textures. Motivated by the interplay between geometry and topology [36–38], we seek a way to geometrically control topological transport. Previous works have investigated geometrical effects in curved low-dimensional magnetic systems, primarily focusing on energetic stabilization of topological spin textures [39–44]. These developments are spurred by advancements in fabrication and imaging techniques for complex magnetic structures [43,45–47].

In this Letter, we study the transport of vorticity on curved magnetic membranes. To this end, we demonstrate that magnetic textures on curved membranes exhibit *topological hydrodynamics*, a transport theory for vortices [48]. This is governed by a robust continuity equation rooted in the homotopic properties of the magnetic order parameter space, rather than any structural symmetries. In contrast to previous studies focused on vortex transport in flat magnetic films [20–22,49], this work leverages the geometry of curved magnetic films to reduce symmetries, thereby enabling processes that are otherwise ruled out on symmetry grounds. Notably, the chirality of the system plays a key role in allowing electric current to energetically bias vorticity injection on the membrane. A potential functionality of this physics is then illustrated by an experimentally feasible energy storage concept. Inspired by thermoelectricity, we derive the dimensionless *vortexoelectric* figure of merit $\mathcal{Z}_v$ as the counterpart to the thermoelectric figure of merit ZT and discuss the thermodynamic efficiency of the battery via this quantity.

Topological continuity equation. The magnetic membrane is a two-dimensional orientable manifold $\mathcal{M}$, parametrized by coordinates ξ^1 and ξ^2, with boundary $\partial\mathcal{M}$. $\mathcal{M}$ is embedded in the Euclidean space $\mathbb{R}^3$ from which it inherits the metric g_{ij}. At every point (ξ^1, ξ^2) on $\mathcal{M}$ and for any time t, we identify a unit normal vector $\mathbf{n}(t, \xi^1, \xi^2)$ and define unit vectors spanning the local tangent plane, $\mathbf{e}_1(t, \xi^1, \xi^2)$ and $\mathbf{e}_2(t, \xi^1, \xi^2)$. The orthonormal triad $\{\mathbf{e}_1, \mathbf{e}_2, \mathbf{n}\}$ is the local frame. $\mathcal{M}$ may smoothly change over time, as long as its topology remains unchanged, i.e., $\mathcal{M}$ is not cut. Figure 1 depicts the simplest case in which $\mathcal{M}$ is homeomorphic to a closed disk.

The U(1) gauge freedom in specifying the local frame, corresponding to simultaneous rotations of $\mathbf{e}_1$ and $\mathbf{e}_2$ about $\mathbf{n}$, translates into the gauge potential [50–52]

$$\mathcal{A}_\mu = \mathbf{e}_1 \cdot \partial_\mu \mathbf{e}_2, \tag{1}$$

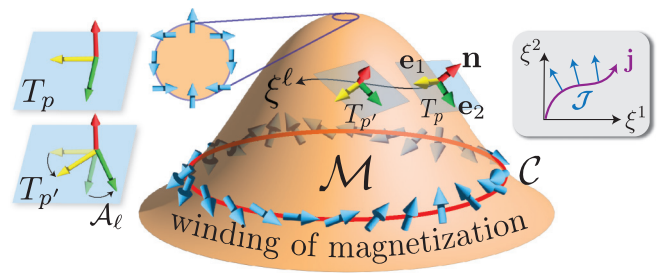

FIG. 1. Depiction of manifold $\mathcal{M}$. The winding of the magnetization $\mathbf{m}$ (blue arrows) on the contour $\mathcal{C}$ (red line) determines the vortex charge enclosed by $\mathcal{C}$. The local tangent planes T_p and $T_{p'}$ are shown for points p and p', along with the local frame $\{\mathbf{e}_1, \mathbf{e}_2, \mathbf{n}\}$. The leftmost tangent planes depict the gauge potential $\mathcal{A}_\ell$ at point p', which captures changes of $\mathbf{e}_1$ and $\mathbf{e}_2$ along ξ^ℓ. The inset shows vorticity flux $\mathcal{J}$ being pumped transverse to a metallic wire (purple curve) carrying electric current density $\mathbf{j}$.

which is a smooth field describing changes of the local frame in space and time. Once the $\mathbf{e}_1$ and $\mathbf{e}_2$ vector fields are specified, the gauge is fixed. The spatial component of the gauge, $\mathcal{A}_i$, is the smooth connection on $\mathcal{M}$, which captures changes in $\mathbf{e}_1$ and $\mathbf{e}_2$ along ξ^i [51]. The gauge-independent field strength tensor stemming from $\mathcal{A}_\mu$ is

$$\mathcal{F}_{\mu\nu} = \partial_\mu \mathcal{A}_\nu - \partial_\nu \mathcal{A}_\mu. \tag{2}$$

We can invoke the Mermin-Ho relation to express the field-strength tensor in terms of the surface normal as $\mathcal{F}_{\mu\nu} = \mathbf{n} \cdot (\partial_\mu \mathbf{n} \times \partial_\nu \mathbf{n})$, making apparent its gauge independence. The "electric" component, $\mathcal{F}_{0i}$, vanishes for static membranes. The "magnetic" component, $\mathcal{F}_{ij}$, relates to the Gaussian curvature $\mathcal{K}$ by $\mathcal{K} = \mathcal{F}_{12}/\sqrt{g}$ [51]. Here, g is the determinant of the metric and the Levi-Civita tensor convention is $\epsilon^{012} = 1$. We make a convention in which Greek indices $\mu = 0, 1, 2 \leftrightarrow t, \xi^1, \xi^2$ label spacetime coordinates and Latin indices $i = 1, 2 \leftrightarrow \xi^1, \xi^2$ label spatial coordinates, while repeated indices are summed over.

We assume the magnetic texture is described by a continuum coarse-grained vector field $\mathbf{m}(t, \xi^1, \xi^2)$ realizing the map $\mathcal{M} \mapsto \mathbb{R}^3$ at all times t. This description holds over a broad temperature range, from order to disorder. In the low-temperature (locally) ordered phase, $\mathbf{m}$ is normalized by its $T = 0$ value and the membrane can be either ferromagnetic or antiferromagnetic. $\mathbf{m}$ is the local spin density in the former case, whereas in the latter case, $\mathbf{m}$ is the local Néel order. In the high-temperature paramagnetic regime, $\mathbf{m}$ may fluctuate in both magnitude and direction. Irrespective of any local fluctuations of $\mathbf{m}$ or dynamics of $\mathcal{M}$, the field $\mathbf{m}$ exhibits topological hydrodynamics governed by the continuity equation $\partial_\mu \mathcal{J}^\mu = 0$, where

$$\mathcal{J}^\mu = \frac{\epsilon^{\mu\nu\rho}}{2\pi}\left[\mathbf{n} \cdot (\boldsymbol{\nabla}_\nu \mathbf{m} \times \boldsymbol{\nabla}_\rho \mathbf{m}) - \frac{1}{2}\mathcal{F}_{\nu\rho}\mathbf{m}_\parallel^2\right], \tag{3}$$

written using the gauge-covariant derivative of $\mathbf{m}$,

$$\boldsymbol{\nabla}_\mu \mathbf{m} \equiv (\partial_\mu m^a)\mathbf{e}_a - \mathcal{A}_\mu(\mathbf{n} \times \mathbf{m}). \tag{4}$$

Here, $\mathbf{m}_\parallel$ is the projection of $\mathbf{m}$ onto the local tangent plane. $\mathcal{J}^\mu = (\mathcal{J}^0, \boldsymbol{\mathcal{J}})$ is the gauge-independent vorticity 3-current, where $\mathcal{J}^0$ is the vorticity density and $\boldsymbol{\mathcal{J}}$ is the vorticity flux. In the absence of curvature and membrane dynamics, the frame can be made constant, so the vorticity 3-current reduces to $\mathcal{J}^\mu = \epsilon^{\mu\nu\rho}\mathbf{n} \cdot (\partial_\nu \mathbf{m} \times \partial_\rho \mathbf{m})/2\pi$ [20,22].

For flat systems, in the limit of an in-plane magnetic texture with fixed magnitude, the field homotopy defined on the boundary dictates the conserved integer vortex charge in the bulk [33]. Whenever a vortex is moved across the boundary, there must be a commensurate change in the winding. Here, the topological continuity equation generalizes these ideas for curved systems with a magnetic texture that can traverse out of plane and fluctuate in magnitude. In contrast, the known skyrmion continuity equation [53] does not derive from such a bulk-boundary correspondence. Hence, skyrmions can locally fluctuate in and out of existence if $|\mathbf{m}|$ is allowed to vary [54]. The continuity equation for vorticity is rooted in topology and is derived independently of the details of the system, thus being immune to any structural imperfections or anisotropies. However, the physical behavior of the system will be highly sensitive to these details [3,55]. In this work, we will focus on systems in which magnetic vorticity may be the natural transport quantity. We consider magnetic membranes with easy-surface anisotropy, namely, there is a local hard anisotropy axis collinear with the surface normal [41,56] that endows the magnetic texture with an XY character [3,57].

Gauge-independent topological charge. To elucidate the bulk-boundary correspondence, we will construct the gauge-independent vortex density in terms of the magnetic winding. It is known that for flat magnetic films, the winding along a curve is $\mathbf{m}_\parallel^2 \partial_\ell \varphi/2\pi$ [20,22,27], with ℓ the arclength. Following this structure, the winding on curved membranes generalizes to the gauge-covariant winding $\mathbf{m}_\parallel^2 D_\ell \varphi/2\pi \equiv \mathbf{m}_\parallel^2(\partial_\ell \varphi - \mathcal{A}_\ell)/2\pi$. Here, φ is the polar in-(tangent)-plane angle of $\mathbf{m}_\parallel$ relative to $\mathbf{e}_1$. For φ to be well defined, we require $|\mathbf{m}_\parallel| > 0$ everywhere on $\mathcal{M}$, except for isolated points. Invoking the generalized Stokes theorem [36,58], the gauge-independent topological charge on a patch $\mathcal{S}$ is

$$\mathcal{Q} = \frac{1}{2\pi}\int_{\partial\mathcal{S}} d\xi^i\, \mathbf{m}_\parallel^2 D_i \varphi = \int_{\mathcal{S}} d\xi^1 d\xi^2\, \mathcal{J}^0. \tag{5}$$

We see that the integrated winding around the boundary $\partial\mathcal{S}$ equals the vorticity density integrated over $\mathcal{S}$. The conserved density $\mathcal{J}^0$ is derived by the exterior derivative of the winding 1-form in the leftmost integral. We expand upon this construction in the Supplemental Material [59].

Even when specializing to the strong easy-surface limit where $|\mathbf{m}_\parallel| = 1$, the topological charge $\mathcal{Q}$ is noninteger-valued if $\mathcal{M}$ has nonzero Gaussian curvature $\mathcal{K}$. In this limit, we can evaluate $\mathcal{Q} = \mathcal{N} - \int_{\mathcal{S}} dS\, \mathcal{K}/2\pi$ for a patch $\mathcal{S}$. This is the difference of an integer $\mathcal{N}$ that counts the number of vortices on $\mathcal{S}$ and a geometric background offset that spoils the discreteness of $\mathcal{Q}$. $\mathcal{N}$ is the S^1 winding number connecting $\mathcal{Q}$ to its homotopic roots. A similar geometry-induced offset to the topological charge also appears when calculating the skyrmion number on curved surfaces [60].

Torsion-enabled pumping of vorticity. Having established a conserved topological charge, we now wish to control it. Suppose we wrap a static magnetic membrane with a metallic wire parametrized by unit tangent vector $\mathbf{v}(\ell)$, with ℓ the arclength, and induce electric current flow in the wire. Following the approach developed in Refs. [20,22], we construct a torque acting on a smooth magnetic texture, which energetically biases vorticity injection transverse to the wire, as depicted in the inset of Fig. 1. This engenders the *vortexoelectric effect*. To enable this process, we use the local torsion of the wire, $\mathfrak{T}(\ell) = \mathbf{v} \cdot (\mathbf{a} \times \partial_\ell \mathbf{a})$, to geometrically reduce symmetries [58]. The torsion is the helical winding of the principal normal vector $\mathbf{a}(\ell) = \partial_\ell \mathbf{v}/|\partial_\ell \mathbf{v}|$ along the wire, and is zero for curves on flat surfaces. This means that for flat magnetic systems, this process would be ruled out on symmetry grounds. Notably, torsion is a pseudoscalar, so $\mathfrak{T}\mathbf{n}$ is a pseudovector with identical spatial properties to magnetization which can be substituted for $\mathbf{M}$ in Refs. [20,22].

The gauge-independent torque is constructed phenomenologically on general symmetry grounds so that the work done on the magnetic texture is proportional to the vorticity flow across the wire. Focusing, for simplicity, on the low-temperature limit where $|\mathbf{m}| = 1$, we require a torque

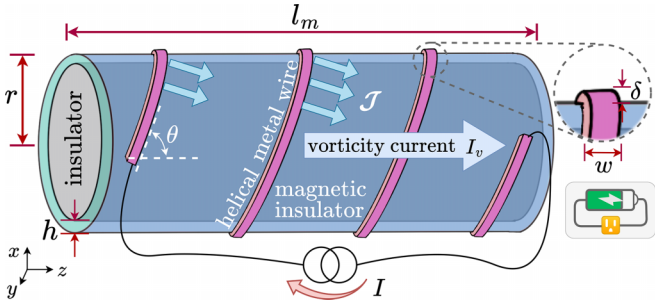

FIG. 2. Schematic of a minimal setup for geometrically controlled vortex transport. A metallic wire is wrapped around a cylindrical magnetic insulator membrane as a helix. An applied electric current I induces vorticity flux $\mathcal{J}$ transverse to the wire, resulting in vorticity current I_v along z. The side panel indicates that this system realizes a battery.

orthogonal to $\mathbf{m}$. A torque (per unit length) that satisfies this is [59]

$$\boldsymbol{\tau} = \frac{\zeta j}{\pi}(\mathfrak{T}\mathbf{n}\cdot\mathbf{m})[\nabla_\ell \mathbf{m} + \mathbf{n}\,\partial_\ell(\mathbf{n}\cdot\mathbf{m})]. \tag{6}$$

Here, $j = \mathbf{j}\cdot\mathbf{v}$ is the electric current density, and ζ is a phenomenological parameter characterizing the geometry-enabled dissipative coupling of electric and vortex dynamics. Importantly, this torque is only permitted in the presence of spin-orbit coupling. This reminds us of the chirality-induced spin selectivity effect, which arises from the coupling of the electron linear momentum to spin degrees of freedom in chiral materials [61,62]. Furthermore, in the limit of strong spin-orbit coupling, dimensional analysis suggests $\zeta \sim \hbar w \lambda_F^2/e$, where λ_F is the Fermi wavelength, e is the positive elementary electric charge, and w is the width of the wire.

The work done on the magnetic texture is

$$\delta W = \int d\ell\, dt\, \boldsymbol{\tau}\cdot(\mathbf{m}\times\partial_t\mathbf{m}) = \zeta\mathfrak{T} j\,\delta\mathcal{Q}, \tag{7}$$

where $\delta\mathcal{Q} = \int dt d\ell\, \mathbf{v}\cdot(\mathcal{J}\times\mathbf{n})$ is the vorticity flow across the wire. The effective vortex chemical potential is $\mu \equiv \delta W/\delta Q = \zeta\mathfrak{T} j$. In the high-temperature paramagnetic regime, a linear relation $\mu \propto j$ should still hold, although thermal fluctuations of $|\mathbf{m}|$ will renormalize the prefactor.

Vortex circuit elements. Figure 2 illustrates a possible setup where torsion gives rise to pumping of vorticity. Here, a magnetic insulating membrane (which can either be ferro- or antiferromagnetic) of thickness h and length l_m wraps around a cylindrical insulating core. A metal wire of width w and thickness δ wraps around the cylindrical magnetic membrane of radius r as a uniform helix with helix angle θ. Systems with similar geometry, in the form of rolled magnetic membranes, have been fabricated [63]. The uniform helix has a constant torsion $\mathfrak{T} = \sin(2\theta)/2r$, allowing electric current flow in the wire to drive a vorticity flux $\mathcal{J}$, which we assume is transverse to the wire. For this setup, the vortex current will flow along the cylinder in the same direction as the electrical current flow, irrespective of the sign of the torsion $\mathfrak{T}$ [64].

$\mathcal{J}$ can be decomposed into components orthogonal and parallel to the z axis. The former accumulates winding along z, which may unwind at the ends of the cylinder. The latter, on the other hand, builds up winding azimuthally, which is energetically protected by the easy-surface anisotropy. We are interested in the vortex current flowing in the z direction, $I_v = 2\pi r|\mathcal{J}|\sin\theta$, which is driven by the vortex motive force $I\mathfrak{R}$ generated by the electric current. Here,

$$\mathfrak{R} = \frac{\zeta\mathfrak{T} l_m}{2\pi r w\delta}\tan\theta \tag{8}$$

is the vortexoelectric drag coefficient, which can be understood as the analog to the Seebeck coefficient [59]. Different from our previous works on energy storage using topological spin textures [19,20], $\mathfrak{R}$ is unique to the nontrivial geometry of this setup and is absent from flat counterparts. Upon substitution of $\mathfrak{T} = \sin(2\theta)/2r$, we find $\mathfrak{R} \propto \sin^2\theta$. In the linear response, $I_v \propto \mathfrak{R}$, so $\theta = \pi/2$ maximizes the vorticity flow.

The membrane behaves like a series R_vC_v circuit in response to nonzero vortex flow, exhibiting an effective vortex resistance R_v and effective winding capacitance C_v. As dictated by the bulk-boundary correspondence, the vortex current "winds up" the magnetic texture, thereby storing exchange energy. The stiffness of the magnetic texture engenders C_v. On the other hand, R_v can arise due to Gilbert damping, defects, and vortex-antivortex collisions. Following Ref. [20], we estimate C_v and R_v by exploiting the duality between the XY magnet and two-dimensional electrostatics [57]. We find

$$C_v = \frac{1}{A}\frac{r}{2\pi h l_m}, \quad R_v = \frac{1}{\sigma_v}\frac{l_m}{2\pi r}, \tag{9}$$

where σ_v^{-1} is the vortex resistivity and A is the magnetic stiffness [59]. With the circuit elements $\mathfrak{R}$, R_v, and C_v in hand, we set out to construct topological circuits [20].

Coupled topological circuits. The setup we have been discussing can be described by coupled vorticity and electric circuits, which are depicted in Fig. 3. The applied electric current I in the wire supplies an effective vortex motive force $I\mathfrak{R}$ to the vorticity circuit. This results in buildup of winding and an effective vortex voltage $V_v = -\mathcal{Q}/C_v$. The backaction of vortex dynamics on the electrical response induces an electromotive force $I_v\mathfrak{R}$ on the electric circuit, which is written down by invoking Onsager reciprocity. Note that, like ordinary charge, vorticity is even under time reversal. Kirchhoff's law for the coupled electrical and vorticity circuits is thus

$$\begin{pmatrix} V \\ V_v \end{pmatrix} = \begin{pmatrix} R + L\frac{d}{dt} & -\mathfrak{R} \\ -\mathfrak{R} & R_v \end{pmatrix}\begin{pmatrix} I \\ I_v \end{pmatrix}. \tag{10}$$

Here, V is the electric voltage, L is the self-inductance, and R is the electrical resistance. The resistance matrix is symmetric as dictated by Onsager reciprocity, and positive-definite according to the second law of thermodynamics [65,66]. The latter constraint enforces $0 < \xi < 1$, where $\xi \equiv \mathfrak{R}^2/RR_v$ parametrizes the relative strength of the off-diagonal to the diagonal elements of the resistance matrix.

Fourier-transforming Eq. (10) into the frequency domain, we find the effective impedance is

$$Z(\omega) \equiv \frac{V(\omega)}{I(\omega)} = R + i\omega L - \frac{i\omega C_v\mathfrak{R}^2}{1 + i\omega C_v R_v}. \tag{11}$$

Similar to conventional RC circuits, here, $\tau = R_vC_v = (4\pi^2 Ah\sigma_v)^{-1}$ is the timescale for loading and discharging vortices from the magnetic texture. In the high-frequency

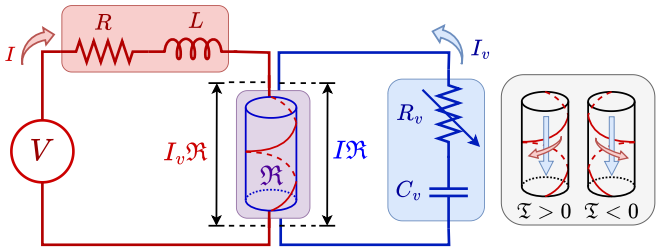

FIG. 3. Schematic of the vorticity (blue) and electric (red) circuits, which are coupled through $\mathfrak{R}$ (purple). $\mathfrak{R}$ gives rise to an effective vortex motive force $I\mathfrak{R}$ on the vorticity circuit and, reciprocally, an electromotive force $I_v\mathfrak{R}$ on the electrical response. R_v is tunable, allowing switching between vortex conducting and insulating regimes. The side panel depicts setups for positive and negative $\mathfrak{T}$, with both electrical and vortex currents flowing downward.

regime, $\omega \gg 1/\tau$, the last term in Eq. (11) approximates $-\mathfrak{R}^2/R_v$. The vorticity circuit reduces the effective resistance of the electrical circuit. In the low-frequency limit, $\omega \ll 1/\tau$, the vorticity circuit acts like an inductor with effective negative inductance $L_v = -C_v\mathfrak{R}^2$. Impedance measurements of the circuit in the low-frequency regime could pave a way to probe the strength of the coupling between vortex and charge currents. Similar impedance measurements on helical-spin magnets have been performed to characterize the current-driven dynamics of spin-helix structures [67].

Energy storage and efficiency. In addition to providing a means to measure ζ, the setup depicted in Fig. 2 may also function as a battery. Operation of the battery requires a mechanism to switch the vortex conductivity between the conducting and insulating regimes, allowing the battery to alternate between (dis)charging and storing energy, respectively. The vortex transport parameters could be very sensitive and may be modulated, for example, by heating and cooling the magnet [20,57].

To charge the battery, we electrically bias vortex flow along z, building up azimuthal spin winding so the magnet accumulates exchange energy. Discharging the battery is the reverse process wherein a vortex current induces an electromotive force on the electric circuit, which we may extract as energy. We store the exchange energy by lowering the vortex conductivity, so vortex transport parameters enter the insulating regime. Once in the insulating regime, the Landau criterion governs the amount of winding we can stabilize since the magnetic bulk cannot host an arbitrarily sharp texture [19,68]. The easy-surface anisotropy ($\sim K$) protects the topological spin texture by energetically preventing "phase-slip" events during which the magnetic order parameter unwinds [69]. Thus, easy-surface anisotropy determines the maximal energy storage capacity, which saturates when winding texture energy $[\sim A(D_\ell\varphi)^2]$ is comparable to K.

The charging and discharging efficiencies may be used to characterize the battery. In the vortex conducting regime, we charge the battery relative to its ground state by supplying a dc electric current I_0 for duration τ. By tuning R_v, we can switch to the vortex insulating regime to store the energy in the winding capacitor. The charging efficiency η_c is the ratio of the stored energy to the total energy supplied by the electric circuit. We extract the stored energy by connecting the battery to a load resistor R_L, then switching back to the vortex conducting regime to discharge. The discharging efficiency η_d is the ratio of energy consumed by R_L to the energy leaving the winding capacitor.

Neglecting the self-inductance L, the efficiencies are

$$\eta_c = \frac{1}{2}\frac{(1-e^{-1})^2}{\mathcal{Z}_v^{-1}+e^{-1}}, \quad \eta_d = \frac{1-\gamma}{1+(\mathcal{Z}_v\gamma)^{-1}}, \tag{12}$$

written with $\gamma = R_L/(R_L+R)$ and $\mathcal{Z}_v \equiv \xi/(1-\xi)$, where $\xi = \mathfrak{R}^2/RR_v$. Here, we define the *vortexoelectric* figure of merit $\mathcal{Z}_v$ by analogy to the thermoelectric figure of merit ZT [70–72]. Whereas for the thermoelectric effect, heat and charge currents are coupled, in this setting, we cross-couple vortex and electric currents. Since $\mathcal{Z}_v$ is a monotonic function of ξ, optimizing the system geometry to maximize $\xi \sim adw\lambda_F^2 \sin^4\theta\cos\theta/hr^3\delta$ maximizes $\mathcal{Z}_v$ and, hence, the efficiencies. Here, d is the electron mean free path and a is the lattice spacing. $\mathcal{Z}_v$ is improved by decreasing r, thinning the membrane and the metal wire by decreasing δ and h, or enlarging the metal-magnet interface by increasing w. The optimal helix angle is $\theta \approx 63^\circ$, which balances maximizing I_v and minimizing energy lost due to Joule heating. In the maximal efficiency limit, $\mathcal{Z}_v \to \infty$, the efficiencies simplify to $\eta_c = (e-1)^2/2e$ and $\eta_d = 1-\gamma$ for (dis)charging times of $t = \tau$. Furthermore, in the short charging time limit of $t/\tau \to 0$, while still having $\mathcal{Z}_v \to \infty$, the charging efficiency saturates as $\eta_c \to 1$.

Discussion. In this work, we developed topological hydrodynamics for vortices on curved membranes and proposed an avenue to use geometric properties of the system, in particular chirality, as a tunable handle to bias vortex transport. To achieve this, we phenomenologically introduced a torque that uses geometric torsion to enable electric current-induced vortex pumping. With these building blocks, we analyzed a minimal setup which is described by an effective coupled electrical-vorticity circuit and realizes a feasible energy storage concept. We derive the vortexoelectric figure of merit $\mathcal{Z}_v$ and use this quantity to characterize the thermodynamic efficiency of the battery.

For future works, we may extend our formalism to manifolds with different topologies, such as the Möbius strip. These setups may potentially be achieved by modern fabrication techniques, which have been employed to manufacture complex magnetic structures [44,63,73,74]. It is important to note that the topological continuity equation we formulated applies not only to magnetic systems but also more broadly to any system with a vectorial order parameter. In particular, these concepts can be directly applied to describe the transport of nematic disclinations in liquid crystals, a topic of much recent interest [75–80]. Another possible direction would be to expand beyond vortex circuit elements and develop logic elements based on this physics.

Acknowledgments. We thank Denys Sheka and Se Kwon Kim for insightful discussions. This work was primarily

supported by the U.S. Department of Energy, Office of Basic Energy Sciences, under Grant No. DE-SC0012190. J.Z. acknowledges the support of the Georg H. Endress Foundation.

[1] J. Zang, V. Cros, and A. Hoffmann, *Topology in Magnetism* (Springer, New York, 2018).
[2] S. Maekawa, S. O. Valenzuela, E. Saitoh, and T. Kimura, *Spin Current* (Oxford University Press, Oxford, 2017).
[3] A. M. Turner, V. Vitelli, and D. R. Nelson, Vortices on curved surfaces, Rev. Mod. Phys. **82**, 1301 (2010).
[4] X. Zhang, Y. Zhou, K. M. Song, T.-E. Park, J. Xia, M. Ezawa, X. Liu, W. Zhao, G. Zhao, and S. Woo, Skyrmion-electronics: Writing, deleting, reading and processing magnetic skyrmions toward spintronic applications, J. Phys.: Condens. Matter **32**, 143001 (2020).
[5] K. Mæland and A. Sudbø, Topological superconductivity mediated by skyrmionic magnons, Phys. Rev. Lett. **130**, 156002 (2023).
[6] S. S. Cherepov, B. C. Koop, A. Y. Galkin, R. S. Khymyn, B. A. Ivanov, D. C. Worledge, and V. Korenivski, Core-core dynamics in spin vortex pairs, Phys. Rev. Lett. **109**, 097204 (2012).
[7] X.-G. Wang, G.-h. Guo, A. Dyrdał, J. Barnaś, V. K. Dugaev, S. S. P. Parkin, A. Ernst, and L. Chotorlishvili, Skyrmion Echo in a system of interacting skyrmions, Phys. Rev. Lett. **129**, 126101 (2022).
[8] S. Dasgupta, S. Zhang, I. Bah, and O. Tchernyshyov, Quantum statistics of vortices from a dual theory of the *xy* ferromagnet, Phys. Rev. Lett. **124**, 157203 (2020).
[9] A. Rana, C.-T. Liao, E. Iacocca, J. Zou, M. Pham, X. Lu, E.-E. C. Subramanian, Y. H. Lo, S. A. Ryan, C. S. Bevis, R. M. Karl, A. J. Glaid, J. Rable, P. Mahale, J. Hirst, T. Ostler, W. Liu, C. M. O'Leary, Y.-S. Yu, K. Bustillo *et al.*, Three-dimensional topological magnetic monopoles and their interactions in a ferromagnetic meta-lattice, Nat. Nanotechnol. **18**, 227 (2023).
[10] E. Schwartz, B. Li, and A. A. Kovalev, Superfluid spin transistor, Phys. Rev. Res. **4**, 023236 (2022).
[11] M. Vogel, B. Zimmermann, J. Wild, F. Schwarzhuber, C. Mewes, T. Mewes, J. Zweck, and C. H. Back, Driving a magnetic texture by magnon currents, Phys. Rev. B **107**, L100409 (2023).
[12] M. Stepanova, J. Masell, E. Lysne, P. Schoenherr, L. Köhler, M. Paulsen, A. Qaiumzadeh, N. Kanazawa, A. Rosch, Y. Tokura, A. Brataas, M. Garst, and D. Meier, Detection of topological spin textures via nonlinear magnetic responses, Nano Lett. **22**, 14 (2022).
[13] S. S. P. Parkin, M. Hayashi, and L. Thomas, Magnetic domain-wall racetrack memory, Science **320**, 190 (2008).
[14] R. Bläsing, A. A. Khan, P. C. Filippou, C. Garg, F. Hameed, J. Castrillon, and S. S. P. Parkin, Magnetic racetrack memory: From physics to the cusp of applications within a decade, Proc. IEEE **108**, 1303 (2020).
[15] R. Tomasello, E. Martinez, R. Zivieri, L. Torres, M. Carpentieri, and G. Finocchio, A strategy for the design of skyrmion racetrack memories, Sci. Rep. **4**, 6784 (2014).
[16] R. Tomasello, V. Puliafito, E. Martinez, A. Manchon, M. Ricci, M. Carpentieri, and G. Finocchio, Performance of synthetic antiferromagnetic racetrack memory: Domain wall versus skyrmion, J. Phys. D **50**, 325302 (2017).
[17] J. Müller, Magnetic skyrmions on a two-lane racetrack, New J. Phys. **19**, 025002 (2017).
[18] R. M. Otxoa, R. Rama-Eiroa, P. E. Roy, G. Tatara, O. Chubykalo-Fesenko, and U. Atxitia, Topologically-mediated energy release by relativistic antiferromagnetic solitons, Phys. Rev. Res. **3**, 043069 (2021).
[19] Y. Tserkovnyak and J. Xiao, Energy storage via topological spin textures, Phys. Rev. Lett. **121**, 127701 (2018).
[20] D. Jones, J. Zou, S. Zhang, and Y. Tserkovnyak, Energy storage in magnetic textures driven by vorticity flow, Phys. Rev. B **102**, 140411(R) (2020).
[21] J. Zou, S. Zhang, and Y. Tserkovnyak, Topological transport of deconfined hedgehogs in magnets, Phys. Rev. Lett. **125**, 267201 (2020).
[22] J. Zou, S. K. Kim, and Y. Tserkovnyak, Topological transport of vorticity in Heisenberg magnets, Phys. Rev. B **99**, 180402(R) (2019).
[23] L. Cornelissen, J. Liu, R. Duine, J. B. Youssef, and B. Van Wees, Long-distance transport of magnon spin information in a magnetic insulator at room temperature, Nat. Phys. **11**, 1022 (2015).
[24] X. S. Wang, A. Qaiumzadeh, and A. Brataas, Current-driven dynamics of magnetic Hopfions, Phys. Rev. Lett. **123**, 147203 (2019).
[25] D. Raftrey and P. Fischer, Field-driven dynamics of magnetic Hopfions, Phys. Rev. Lett. **127**, 257201 (2021).
[26] Y. Liu, W. Hou, X. Han, and J. Zang, Three-dimensional dynamics of a magnetic Hopfion driven by spin transfer torque, Phys. Rev. Lett. **124**, 127204 (2020).
[27] Y. Tserkovnyak, J. Zou, S. K. Kim, and S. Takei, Quantum hydrodynamics of spin winding, Phys. Rev. B **102**, 224433 (2020).
[28] Y. Tserkovnyak and J. Zou, Quantum hydrodynamics of vorticity, Phys. Rev. Res. **1**, 033071 (2019).
[29] S. Zhang and Y. Tserkovnyak, Antiferromagnet-based neuromorphics using dynamics of topological charges, Phys. Rev. Lett. **125**, 207202 (2020).
[30] C. Psaroudaki and C. Panagopoulos, Skyrmion qubits: A new class of quantum logic elements based on nanoscale magnetization, Phys. Rev. Lett. **127**, 067201 (2021).
[31] J. Xia, X. Zhang, X. Liu, Y. Zhou, and M. Ezawa, Universal quantum computation based on nanoscale skyrmion helicity qubits in frustrated magnets, Phys. Rev. Lett. **130**, 106701 (2023).
[32] J. Zou, S. Bosco, B. Pal, S. S. P. Parkin, J. Klinovaja, and D. Loss, Quantum computing on magnetic racetracks with flying domain wall qubits, Phys. Rev. Res. **5**, 033166 (2023).
[33] N. D. Mermin, The topological theory of defects in ordered media, Rev. Mod. Phys. **51**, 591 (1979).
[34] E. A. Stepanov, C. Dutreix, and M. I. Katsnelson, Dynamical and reversible control of topological spin textures, Phys. Rev. Lett. **118**, 157201 (2017).
[35] C. Chappert, A. Fert, and F. N. Van Dau, The emergence of spin electronics in data storage, Nat. Mater. **6**, 813 (2007).

[36] M. Nakahara, *Geometry, Topology and Physics* (CRC Press, Boca Raton, 2018).

[37] J. C. Baez and J. P. Muniain, *Gauge Fields, Knots and Gravity* (World Scientific Publishing Company, 1994).

[38] T. Frankel, *The Geometry of Physics: An Introduction* (Cambridge University Press, Cambridge, 2011).

[39] D. Makarov and D. D. Sheka, *Curvilinear Micromagnetism: From Fundamentals to Applications* (Springer Nature, 2022).

[40] D. Makarov, O. M. Volkov, A. Kákay, O. V. Pylypovskyi, B. Budinská, and O. V. Dobrovolskiy, New dimension in magnetism and superconductivity: 3D and curvilinear nanoarchitectures, Adv. Mater. **34**, 2101758 (2022).

[41] R. Streubel, P. Fischer, F. Kronast, V. P. Kravchuk, D. D. Sheka, Y. Gaididei, O. G. Schmidt, and D. Makarov, Magnetism in curved geometries, J. Phys. D: Appl. Phys. **49**, 363001 (2016).

[42] M.-C. Wang, C.-C. Huang, C.-H. Cheung, C.-Y. Chen, S. G. Tan, T.-W. Huang, Y. Zhao, Y. Zhao, G. Wu, Y.-P. Feng, H.-C. Wu, and C.-R. Chang, Prospects and opportunities of 2D van der Waals magnetic systems, Ann. Phys. **532**, 1900452 (2020).

[43] D. Sanz-Hernández, A. Hierro-Rodriguez, C. Donnelly, J. Pablo-Navarro, A. Sorrentino, E. Pereiro, C. Magén, S. McVitie, J. M. de Teresa, S. Ferrer, P. Fischer, and A. Fernández-Pacheco, Artificial double-helix for geometrical control of magnetic chirality, ACS Nano **14**, 8084 (2020).

[44] D. D. Sheka, O. V. Pylypovskyi, O. M. Volkov, K. V. Yershov, V. P. Kravchuk, and D. Makarov, Fundamentals of curvilinear ferromagnetism: Statics and dynamics of geometrically curved wires and narrow ribbons, Small **18**, 2105219 (2022).

[45] A. Fernández-Pacheco, R. Streubel, O. Fruchart, R. Hertel, P. Fischer, and R. P. Cowburn, Three-dimensional nanomagnetism, Nat. Commun. **8**, 15756 (2017).

[46] C. Donnelly, A. Hierro-Rodríguez, C. Abert, K. Witte, L. Skoric, D. Sanz-Hernández, S. Finizio, F. Meng, S. McVitie, J. Raabe, D. Suess, R. Cowburn, and A. Fernández-Pacheco, Complex free-space magnetic field textures induced by three-dimensional magnetic nanostructures, Nat. Nanotechnol. **17**, 136 (2022).

[47] C. Donnelly, M. Guizar-Sicairos, V. Scagnoli, S. Gliga, M. Holler, J. Raabe, and L. J. Heyderman, Three-dimensional magnetization structures revealed with x-ray vector nanotomography, Nature (London) **547**, 328 (2017).

[48] Y. Tserkovnyak, Perspective: (Beyond) spin transport in insulators, J. Appl. Phys. **124**, 190901 (2018).

[49] M. Tanhayi Ahari, S. Zhang, J. Zou, and Y. Tserkovnyak, Biasing topological charge injection in topological matter, Phys. Rev. B **104**, L201401 (2021).

[50] J. Schwichtenberg, Demystifying gauge symmetry, arXiv:1901.10420.

[51] R. D. Kamien, The geometry of soft materials: A primer, Rev. Mod. Phys. **74**, 953 (2002).

[52] A. Zee, *Quantum Field Theory in a Nutshell* (Princeton University Press, 2003).

[53] N. Papanicolaou and T. Tomaras, Dynamics of magnetic vortices, Nucl. Phys. B **360**, 425 (1991).

[54] K. Everschor-Sitte, J. Masell, R. M. Reeve, and M. Kläui, Perspective: Magnetic skyrmions—overview of recent progress in an active research field, J. Appl. Phys. **124**, 240901 (2018).

[55] V. Vitelli and A. M. Turner, Anomalous coupling between topological defects and curvature, Phys. Rev. Lett. **93**, 215301 (2004).

[56] Y. Gaididei, V. P. Kravchuk, and D. D. Sheka, Curvature effects in thin magnetic shells, Phys. Rev. Lett. **112**, 257203 (2014).

[57] J. M. Kosterlitz and D. J. Thouless, Ordering, metastability and phase transitions in two-dimensional systems, J. Phys. C **6**, 1181 (1973).

[58] M. Stone and P. Goldbart, *Mathematics for Physics: A Guided Tour for Graduate Students* (Cambridge University Press, Cambridge, 2009).

[59] See Supplemental Material at http://link.aps.org/supplemental/10.1103/PhysRevB.111.L100401 for (i) the construction of the gauge-independent topological charge, (ii) the differential geometric formulation of topological hydrodynamics, (iii) a derivation of the torsion of a uniform helix, (iv) a discussion on how the phenomenological torque is constructed, and (v) a discussion on how R_v, C_v, and $\mathfrak{R}$ are estimated.

[60] V. P. Kravchuk, U. K. Rößler, O. M. Volkov, D. D. Sheka, J. van den Brink, D. Makarov, H. Fuchs, H. Fangohr, and Y. Gaididei, Topologically stable magnetization states on a spherical shell: Curvature-stabilized skyrmions, Phys. Rev. B **94**, 144402 (2016).

[61] R. Naaman and D. H. Waldeck, Chiral-induced spin selectivity effect, J. Phys. Chem. Lett. **3**, 2178 (2012).

[62] S. Dalum and P. Hedegård, Theory of chiral induced spin selectivity, Nano Lett. **19**, 5253 (2019).

[63] R. Streubel, F. Kronast, P. Fischer, D. Parkinson, O. G. Schmidt, and D. Makarov, Retrieving spin textures on curved magnetic thin films with full-field soft x-ray microscopies, Nat. Commun. **6**, 7612 (2015).

[64] Electrical current flow in the z direction will generically drag an additional vortex current, since vortices and antivortices are not related by structural symmetries, thus having distinct physical properties. For example, antivortices could be immobile while vortices are not. We expect this drag effect to be insensitive to the sign of the torsion $\mathfrak{T}$, as well.

[65] L. Onsager, Reciprocal relations in irreversible processes. I., Phys. Rev. **37**, 405 (1931).

[66] I. Gyarmati *et al.*, *Non-Equilibrium Thermodynamics* (Springer, 1970).

[67] T. Yokouchi, F. Kagawa, M. Hirschberger, Y. Otani, N. Nagaosa, and Y. Tokura, Emergent electromagnetic induction in a helical-spin magnet, Nature (London) **586**, 232 (2020).

[68] E. Sonin, Spin currents and spin superfluidity, Adv. Phys. **59**, 181 (2010).

[69] S. K. Kim, S. Takei, and Y. Tserkovnyak, Thermally activated phase slips in superfluid spin transport in magnetic wires, Phys. Rev. B **93**, 020402(R) (2016).

[70] A. Majumdar, Thermoelectricity in semiconductor nanostructures, Science **303**, 777 (2004).

[71] A. A. Kovalev and Y. Tserkovnyak, Magnetocaloritronic nanomachines, Solid State Commun. **150**, 500 (2010).

[72] G. E. W. Bauer, S. Bretzel, A. Brataas, and Y. Tserkovnyak, Nanoscale magnetic heat pumps and engines, Phys. Rev. B **81**, 024427 (2010).

[73] C. Phatak, Y. Liu, E. B. Gulsoy, D. Schmidt, E. Franke-Schubert, and A. Petford-Long, Visualization of the magnetic structure of sculpted three-dimensional cobalt nanospirals, Nano Lett. **14**, 759 (2014).

[74] L. Skoric, D. Sanz-Hernández, F. Meng, C. Donnelly, S. Merino-Aceituno, and A. Fernández-Pacheco, Layer-by-layer

growth of complex-shaped three-dimensional nanostructures with focused electron beams, Nano Lett. **20**, 184 (2020).

[75] F. Vafa, D. R. Nelson, and A. Doostmohammadi, Periodic orbits, pair nucleation, and unbinding of active nematic defects on cones, Phys. Rev. E **109**, 064606 (2024).

[76] F. Vafa, D. R. Nelson, and A. Doostmohammadi, Active topological defect absorption by a curvature singularity, J. Phys.: Condens. Matter **35**, 425101 (2023).

[77] M. Jiang, Y. Guo, J. V. Selinger, O. D. Lavrentovich, and Q.-H. Wei, Designing, generating and reconfiguring disclination interconnects in nematic liquid crystals, Liq. Cryst. **50**, 1517 (2023).

[78] G. Duclos, R. Adkins, D. Banerjee, M. S. E. Peterson, M. Varghese, I. Kolvin, A. Baskaran, R. A. Pelcovits, T. R. Powers, A. Baskaran, F. Toschi, M. F. Hagan, S. J. Streichan, V. Vitelli, D. A. Beller, and Z. Dogic, Topological structure and dynamics of three-dimensional active nematics, Science **367**, 1120 (2020).

[79] J. C. Everts and M. Ravnik, Ionically charged topological defects in nematic fluids, Phys. Rev. X **11**, 011054 (2021).

[80] J. J. Sandford O'Neill, P. S. Salter, M. J. Booth, S. J. Elston, and S. M. Morris, Electrically-tunable positioning of topological defects in liquid crystals, Nat. Commun. **11**, 2203 (2020).